

Active Ran regulates anillin function during cytokinesis

Daniel Beaudet^{a,†}, Tara Akhshi^{b,c,†}, Julia Philipp^a, Christopher Law^d, and Alisa Piekny^{a,*}

^aDepartment of Biology and ^dCentre for Microscopy and Cellular Imaging, Concordia University, Montreal, QC H4B 1R6, Canada; ^bProgram in Cell Biology, the Hospital for Sick Children, Toronto, ON M5G 0A4, Canada;

^cDepartment of Biochemistry, University of Toronto, Toronto, ON M5S 1A8, Canada

ABSTRACT Cytokinesis cleaves a cell into two daughters at the end of mitosis, and must be spatially coordinated with chromosome segregation to prevent aneuploidy. The dogma is that the mitotic spindle governs the assembly and constriction of an actomyosin ring. Here, we reveal a function for active Ran in spatially restricting the ring. Our model is that during anaphase, “free” importins, whose gradient inversely correlates with active Ran and chromatin position, function as a molecular ruler for the recruitment and localization of anillin, a contractile protein and a crucial regulator of cytokinesis. We found that decreasing Ran-GTP levels or tethering active Ran to the equatorial membrane affects anillin’s localization and causes cytokinesis phenotypes. Anillin contains a conserved nuclear localization signal (NLS) at its C-terminus that binds to importin- β and is required for cortical polarity and cytokinesis. Mutating the NLS decreases anillin’s cortical affinity, causing it to be more dominantly regulated by microtubules. Anillin contains a RhoA-GTP binding domain, which autoinhibits the NLS and the neighboring microtubule-binding domain, and RhoA-GTP binding may relieve this inhibition during mitosis. Retention of the C-terminal NLS in anillin homologues suggests that this is a conserved mechanism for controlling anillin function.

Monitoring Editor

Karsten Weis
ETH Zurich

Received: Apr 20, 2017

Revised: Sep 6, 2017

Accepted: Sep 13, 2017

This article was published online ahead of print in MBoc in Press (<http://www.molbiolcell.org/cgi/doi/10.1091/mbc.E17-04-0253>) on September 20, 2017.

[†]These authors contributed equally to this work.

Author contributions: A.P. wrote the original manuscript and conceptualized and designed the methodology for experiments; T.K.A. and D.B. also helped design methodology and perform experiments, as well as helping to edit the manuscript; D.B. validated experiments performed by T.K.A.; J. P. also performed experiments; T.K.A., D.B., and J.P. formally analyzed the data; C.L. wrote a macro for ImageJ for formal analysis; A.P., T.K.A., and D.B. helped visualize the data in figure format; A.P. and D.B. carried out supervision.

*Address correspondence to: Alisa Piekny (alisa.piekny@concordia.ca).

Abbreviations used: AHD, anillin homology domain; a.u., arbitrary units; BHK, baby hamster kidney cells; Cdk1, cyclin-dependent kinase 1; C-term, carboxyl-terminus; DAPI, 4',6-diamidino-2'-phenylindole dihydrochloride; FL, full-length; GEF, guanine nucleotide exchange factor; GFP, green fluorescent protein; Imp- β , importin- β ; Inh, inhibition; MBP, maltose binding protein; Mem-Ran, mCherry:neuromodulin(1-60) Ran; MLC, myosin light chain; MT, microtubule; M.W., molecular weight; NLS, nuclear localization signal; n.s., not significant; N-term, NH₂-terminus; PH, pleckstrin homology; RBD, RhoA-GTP binding domain; RNAi, RNA interference; ROI, region of interest; ts, temperature sensitive; tsBN2, BHK cells with a ts mutation in RCC1 (Ran GEF).

© 2017 Beaudet, Akhshi, et al. This article is distributed by The American Society for Cell Biology under license from the author(s). Two months after publication it is available to the public under an Attribution-NonCommercial-Share Alike 3.0 Unported Creative Commons License (<http://creativecommons.org/licenses/by-nc-sa/3.0>).

“ASCB®”, “The American Society for Cell Biology®”, and “Molecular Biology of the Cell®” are registered trademarks of The American Society for Cell Biology.

INTRODUCTION

Cytokinesis is driven by the ingression of an actomyosin ring, which cleaves a cell into two daughters. The contractile ring is spatially controlled by the mitotic spindle to coordinate with the segregation of chromosomes and cell fate determinants (Green *et al.*, 2012; Akhshi *et al.*, 2014; D’Avino *et al.*, 2015; Cheffings *et al.*, 2016). Failed or dysfunctional cytokinesis causes changes in cell fate and ploidy, which can be detrimental and/or cause cancer (Lacroix and Maddox, 2012; D’Avino *et al.*, 2015). During early anaphase, actomyosin filaments accumulate at a broad region of the cortex, which transitions into a tight ring-like organization as the cell progresses through mitosis (Green *et al.*, 2012; Akhshi *et al.*, 2014; D’Avino *et al.*, 2015; Cheffings *et al.*, 2016). The highly conserved protein anillin is a crucial regulator of cytokinesis in metazoans and has binding sites for key regulators and core effectors of cytokinesis, including F-actin, myosin, RhoA, septins, phospholipids, and microtubules (Piekny and Maddox, 2010; Tse *et al.*, 2011; van Oostende Triplet *et al.*, 2014). Owing to its ability to bind to these components, previous studies have focused on how inputs from different pathways are integrated by anillin to spatially control the contractile ring (e.g., Zanin *et al.*, 2013; van Oostende Triplet *et al.*, 2014).

Multiple pathways regulate cytokinesis, yet the requirement for them varies between organisms and cell types. The majority of studies have focused on microtubule-dependent mechanisms, for which the prevailing dogma in the field is that the anaphase spindle determines the division plane for cytokinesis. The central spindle stimulates contractile ring assembly around the equatorial cortex (Somers and Saint, 2003; Bement *et al.*, 2005; Yüce *et al.*, 2005; Zhao and Fang, 2005), while astral microtubules exclude contractile proteins from the poles (Dechant and Glotzer, 2003; Bringmann and Hyman, 2005; Werner *et al.*, 2007; Lewellyn *et al.*, 2010; van Oostende Triplet *et al.*, 2014). However, signals from other cellular locations, such as kinetochores, chromatin, or centrosomes, also influence the localization of contractile proteins (e.g., Canman *et al.*, 2000, 2003; Potapova *et al.*, 2006; Deng *et al.*, 2007; Petronczki *et al.*, 2007; Silverman-Gavrila *et al.*, 2008; Cabernard *et al.*, 2010; Kotadia *et al.*, 2012; Dehapiot *et al.*, 2013; Kiyomitsu and Cheeseman, 2013; Zanin *et al.*, 2013; Rodrigues *et al.*, 2015). A kinetochore pathway functions in *Drosophila* and human cells to mediate relaxation of the polar cortex during anaphase, independent of microtubules and centrosomes (Rodrigues *et al.*, 2015). A kinetochore-tethered complex containing PP1 phosphatase and its regulatory subunit Sds22 dephosphorylates the actin regulator moesin at the cell poles to promote cortical relaxation (Carreno *et al.*, 2008; Roubinet *et al.*, 2011; Rodrigues *et al.*, 2015). Although the balance of active moesin is important, it is not essential for cytokinesis per se, and this pathway functions for just a short time during early anaphase. Microtubule-independent pathways may be crucial for cytokinesis in cells where the spindle is positioned far from parts of the cortex, such as in highly polarized cells. In support of this, the cortex still polarizes and ingresses in the absence of polymerized microtubules or an intact mitotic spindle in dividing *Drosophila* neuroblasts with apical/basal polarity (e.g., Cabernard *et al.*, 2010).

Chromatin-associated signals also regulate the cortex during cytokinesis. In yeast and metazoans, a NoCut pathway regulates the abscission machinery to prevent the cortex from cutting through unsegregated chromosomes (Norden *et al.*, 2006; Mendoza *et al.*, 2009; Steigemann *et al.*, 2009). Acetyltransferase is associated with chromatin and regulates the activity of Ipl1/Aurora B kinase to modulate proteins that control abscission, such as Boi1 and Boi2 (anillin-like proteins) and septins in yeast, or MKLP1 in human cells (Norden *et al.*, 2006; Potapova *et al.*, 2006; Mendoza *et al.*, 2009; Steigemann *et al.*, 2009). However, the mechanisms by which chromatin-associated signals regulate the cortex during earlier stages of mitotic exit are not well-understood. In *Drosophila* neuroblasts, increasing the length of chromatid arms causes an increase in the breadth of active myosin localization during late anaphase and early telophase, leading to dramatic changes in cell shape (Kotadia *et al.*, 2012). During meiosis of mouse oocytes, chromatin positioned near the cortex induces the formation of an actin cap via Ran-GTP, and the placement of DNA-coated beads near the cortex induces cortical polarity independent of microtubules (Deng *et al.*, 2007). These studies suggest that a chromatin-associated Ran-GTP gradient functions as a molecular ruler to organize the cortex. Furthermore, this gradient may regulate active Cdc42 and Rac for actin cap formation, while excluding ERM (Ezrin/Radixin/Moesin; Dehapiot *et al.*, 2013; Dehapiot and Halet, 2013). However, it is not clear whether this mechanism applies to cytokinesis, where Cdc42 and Rac are not essential. In another study, Ran-GTP was shown to positively regulate the actomyosin cortex for pseudocleavage furrowing in the early *Drosophila* embryo (Silverman-Gavrila *et al.*, 2008). Ran-GTP releases importin(s) from a nuclear localization signal (NLS) that overlaps with the septin-binding site in the C-terminus of anillin to permit septin binding

(Silverman-Gavrila *et al.*, 2008). It is not clear how this model applies to cytokinesis, because the contractile ring assembles and ingresses away from chromosomes. Another study showed that Ran-GTP inhibits rather than promotes anillin's cortical localization in mitotic mammalian cells (Kiyomitsu and Cheeseman, 2013). While anillin clears from the cortex near chromatin in cells with depolymerized microtubules and induced to exit mitosis, it fails to clear in cells with decreased active Ran (Kiyomitsu and Cheeseman, 2013). The authors suggest a model where Ran-GTP regulates cell elongation in response to chromatin in order to maintain the division plane during cytokinesis (Kiyomitsu and Cheeseman, 2013). However, they did not study the function of Ran-GTP during cytokinesis or the molecular mechanism by which Ran-GTP regulates the cortex.

Here, we show that human anillin is regulated by active Ran during anaphase. We found that decreasing Ran-GTP leads to the ectopic localization of anillin and myosin to the cell poles and blocks furrowing in BHK (baby hamster kidney) epithelial cells. In HeLa cells, targeting active Ran to the furrow membrane causes a reduction in anillin localization and oscillation phenotypes similar to those observed after anillin depletion. Anillin contains a highly conserved NLS at its C-terminus that binds to importin- β , and is needed to mediate cortical polarization and cytokinesis. Furthermore, mutating the NLS reduces anillin's affinity for the equatorial cortex, causing it to be more dominantly regulated by astral microtubules during cytokinesis. However, high overexpression of importin- β negatively regulates anillin's cortical localization. Thus, "free" importins may function as a molecular ruler, for which optimal levels mediate the cortical recruitment of anillin by stabilizing a conformation that improves accessibility to cortical proteins and lipids. However, high levels of importins could reduce off-rates and sterically hinder binding to other sites at the C-terminus. Interestingly, anillin's RhoA-GTP binding domain blocks accessibility to the NLS and the neighboring microtubule-binding domain, and we propose that RhoA-GTP binding during early mitotic exit relieves this autoinhibition. Thus, our model is that RhoA-GTP binding to anillin opens the conformation of the C-terminus to make it more accessible for binding to importin and microtubules. A gradient of free importins forms in response to chromatin, where Ran-GTP levels are high. Optimal levels of importins likely form near the equatorial plane and facilitate anillin's cortical recruitment during anaphase. These results shed light on a novel mechanism through which Ran-GTP polarizes the cortex during cytokinesis.

RESULTS

Active Ran spatially regulates cytokinesis

Recent studies have shown that there is a correlation between chromatin position and the localization of cytokinesis proteins (Rodrigues *et al.*, 2015). During mitosis, Ran-GTP forms a gradient around chromatin that regulates proteins required for bipolar spindle assembly (Kaláb *et al.*, 2002, 2006; Clarke and Zhang, 2008). This gradient persists into anaphase and we propose that it influences the cortex (Li and Zheng, 2004; Lee *et al.*, 2012). To test the role of Ran in cytokinesis, we determined how decreasing the level of endogenous active Ran affects the localization of contractile proteins in tsBN2 cells, which contain a ts mutant of RCC1 (Ran GEF) in BHK epithelial cells (Nishimoto *et al.*, 1978). A reduction in Ran-GTP occurs within minutes of up-shift to a restrictive temperature (39.7°C), and all of our analyses were done after cells were up-shifted for 30–40 min (Lee *et al.*, 2012). Longer up-shifts were detrimental and prevented cells from exiting mitosis, likely due to spindle defects (Kaláb *et al.*, 2002, 2006). A significant proportion of tsBN2 cells, 59% for GFP:anillin and 35% for GFP:myosin (MLC, myosin light chain; active), failed to ingress when up-shifted to a restrictive temperature in comparison

with tsBN2 cells at a permissive temperature (33°C; 0% for GFP:anillin or GFP:myosin) or BHK cells at either temperature (0% at 39.7 or 33°C for anillin:GFP; Figure 1A and Supplemental Figure S1A). To ensure that the mitotic spindle formed properly in the up-shifted cells, we labeled microtubules with Sir-tubulin (in red; Figure 1A). Anillin and myosin appeared to be ectopically recruited to regions outside the equatorial plane, so we measured their cortical accumulation. To do this, a line scan was drawn around the perimeter of the cell and the pixels above 50% maximum levels were summed and calculated as a ratio to the total perimeter (Figure 1B and Supplemental Figure S1A). In tsBN2 cells at a restrictive temperature, the ratio of cortical endogenous anillin and GFP:myosin was greater than in cells at a permissive temperature (Figure 1B and Supplemental Figure S1A). Therefore, decreasing Ran-GTP levels during mitosis causes contractile proteins to be ectopically recruited, likely blocking furrow ingression due to altered cortical properties at the cell poles. However, there is always the caveat that these phenotypes are caused indirectly by spindle perturbations, which can occur when Ran-GTP levels are insufficient. In addition, these phenotypes could be caused by the presence of cortical regulators that should be sequestered in the nucleus, because a reduction in Ran-GTP prevents nuclear envelope reformation (Clarke and Zhang, 2008).

To test whether there is a more direct role for Ran-GTP in regulating cytokinesis, we targeted active Ran to the cleavage furrow membrane. Ran or constitutively active Ran (Q69L) tagged with mCherry were targeted to the equatorial membrane in cells stably expressing anillin:GFP using the phosphatidylinositol 4,5-bisphosphate (PI_{4,5}P₂)-binding domain of neuromodulin (1–60aa; Liu *et al.*, 2012). Cytokinesis phenotypes were observed in cells strongly overexpressing active Ran (fluorescence intensity 1500–3000 a.u.), which were separated into categories of weak cortical instability, such as blebbing or ruffling (39%), and oscillation (35%), where the furrow failed to remain stably positioned (Figure 2A). Cells weakly overexpressing active Ran (460–1500 a.u.) also displayed weak cortical instability (54%), while only a small proportion of cells strongly overexpressing Ran displayed weak cortical instability (23%; Figure 2A). Furrow oscillation and cortical instability are reminiscent of the phenotypes reported for anillin depletion in HeLa cells (Straight *et al.*, 2005; Piekny and Glotzer, 2008), suggesting that active Ran negatively regulates anillin function. We also determined if the overexpression of Ran or Ran (Q69L) is sufficient to cause phenotypes without being targeted to the membrane (Supplemental Figure S1B). No cytokinesis phenotypes were observed in cells overexpressing GFP:Ran or GFP:Ran (Q69L). However, there may be a mild increase in the breadth of anillin in cells overexpressing active Ran (Supplemental Figure S1B). To determine whether membrane-targeted active Ran affects anillin localization, we measured the ratio of cortically accumulated anillin to cytosol (Supplemental Figure S1C) and the ratio of anillin breadth to cell perimeter just prior to furrow ingression (Figure 2B; Zanin *et al.*, 2013). There was no significant change in the total levels of cortical anillin in membrane-targeted active Ran versus Ran or control cells (Supplemental Figure S1C). However, there was a significant increase in the breadth of anillin in the equatorial plane in cells where membrane-targeted active Ran was highly overexpressed (Figure 2B). These data suggest that there is less anillin in the equatorial plane in cells expressing membrane-targeted active Ran. Therefore, targeting active Ran to the membrane may cause insufficient levels of anillin to persist in the equatorial plane to stabilize the ring. To ensure that membrane-targeted Ran overlapped with anillin, we measured colocalization between Ran and anillin in cells at the onset of furrow ingression, which ranged from 40–98% for Ran and Ran (Q69L; Supplemental Figure S1D).

Anillin is a target of the Ran pathway

To find a target of the Ran pathway, we determined which of the known regulators of cytokinesis are needed to polarize the cortex in response to chromatin. First, we verified that Ran polarizes the cortex in HeLa cells lacking polymerized microtubules and induced to exit mitosis (Kiyomitsu and Cheeseman, 2013). HeLa cells display cortical contractility after treatment with 100 nM nocodazole for 3–4 h to depolymerize microtubules, followed by 22.5 μM Purvalanol A to inhibit Cdk1 activity and promote mitotic exit (e.g., Supplemental Figure S2A and Figure 3A; Petronczki *et al.*, 2007). Contractile proteins accumulate around the region of the cortex furthest from chromatin, causing cells to polarize. This polarization is reminiscent of that in monopolar cells treated with S-trityl-L-cysteine (STC) to block centrosome separation and forced to exit mitosis (Supplemental Figure S2A; Hu *et al.*, 2008). To show that cortical polarity is influenced by Ran, HeLa cells lacking polymerized microtubules and induced to exit mitosis were treated with 100 nM Importazole, which was previously shown to disrupt Ran-GTP-importin binding (Supplemental Figure S2B; Soderholm *et al.*, 2011). Cells were assayed for polarization by measuring asymmetric anillin distribution. Anillin was determined to be asymmetric if the ratio (R) of accumulated anillin around part of the cortex, perpendicular to the axis of chromatin position, deviated from the other part by $R > 1.2$ (see schematic in Figure 3A). Indeed, while anillin was asymmetric in 53% of control cells, it was not asymmetrically distributed in the majority of Importazole-treated cells (14%; Supplemental Figure S2B), consistent with previous studies showing that the Ran pathway influences the localization of contractile proteins during mitotic exit (Kiyomitsu and Cheeseman, 2013).

Next, we monitored changes in cortical polarization after cells were treated with different small interfering RNAs (siRNAs) or drugs to deplete or inhibit known cytokinesis regulators (Supplemental Figure S2C). Depleting Ect2 blocked the cortical recruitment of anillin:GFP, consistent with its requirement to generate active RhoA for contractile ring assembly (5% asymmetric vs. 61% control; Yüce *et al.*, 2005). Inhibiting myosin with Blebbistatin had no effect on polarization and anillin:GFP localized asymmetrically in response to chromatin (62% when Blebbistatin was added “early” with Purvalanol A, and 68% when Blebbistatin was added “late” ~7 min after Purvalanol A; Supplemental Figure S2C). However, in anillin-depleted cells, myosin and RhoA were globally localized regardless of chromatin position, and the majority of cells failed to polarize (10 and 3%, respectively, vs. 56% GFP:myosin and 65% GFP:RhoA; Supplemental Figure S2C). Asymmetric anillin distribution and cortical polarization were restored in anillin-depleted cells coexpressing GFP-tagged RNA interference (RNAi)-resistant full length (FL) or C-terminus (C-term) of anillin (75% for endogenous anillin and 9% after anillin RNAi vs. 64% for anillin RNAi + FL anillin (1–1087), and 67% for anillin RNAi + C-term (608–1087); Figure 3, A and B), suggesting that anillin’s N-terminal actin and myosin binding sites are not needed for polarization. These data show that the cortical polarization of cells lacking polymerized microtubules is regulated by anillin or upstream regulators of anillin, as shown in the schematic in Supplemental Figure S2D.

We determined the molecular mechanism by which anillin mediates polarization in response to Ran-GTP. Human anillin contains a NLS at its C-terminus, but this site has not been extensively studied (Oegema *et al.*, 2000). A NLS at the C-terminus of *Drosophila* anillin overlaps with a putative septin-binding region and was shown to bind to importins *in vitro* (Silverman-Gavrila *et al.*, 2008). It was hypothesized that importins released in the vicinity of chromatin-associated Ran-GTP during cellularization permit anillin to form a functional complex

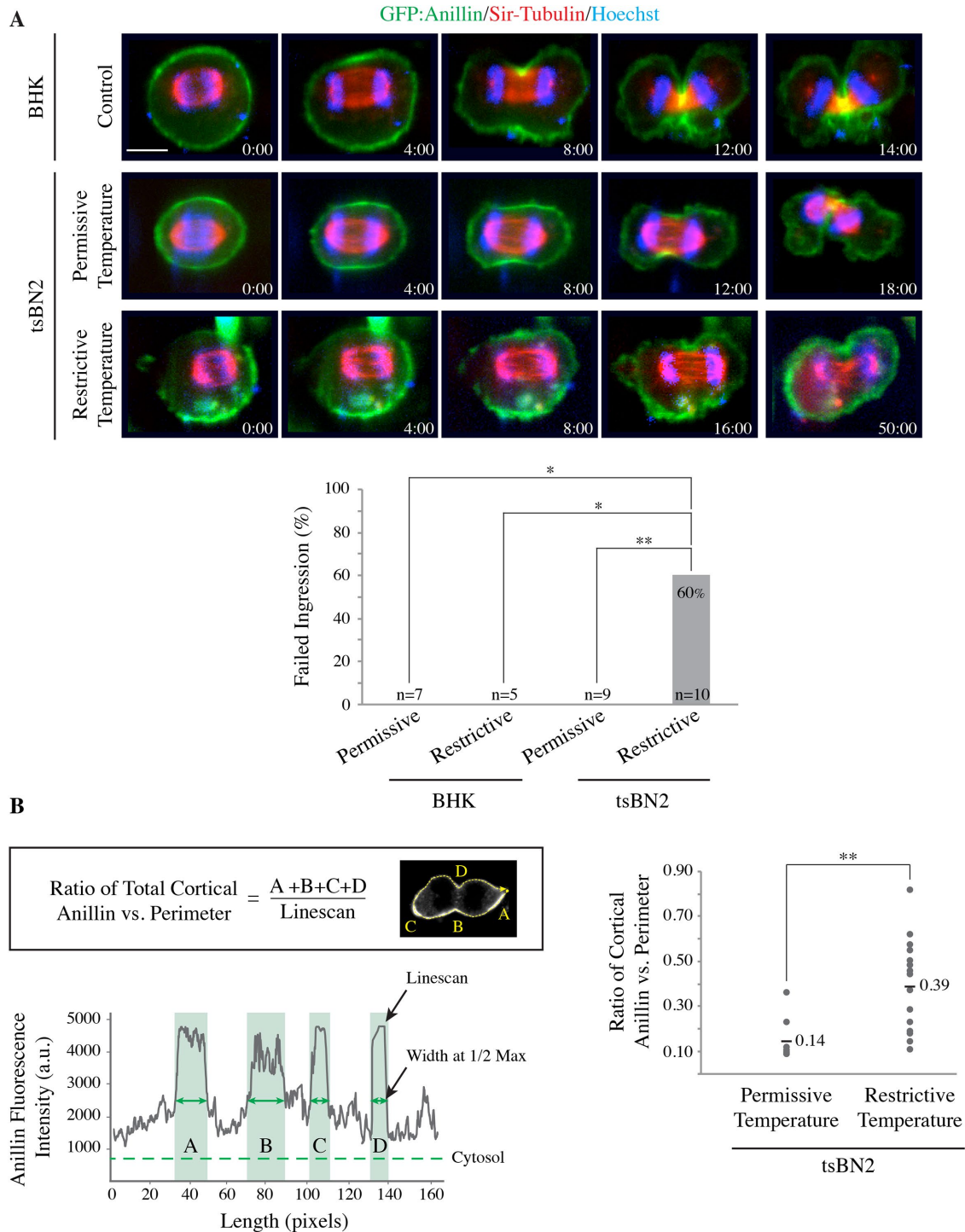


FIGURE 1: Reducing active Ran affects the localization of contractile proteins during cytokinesis. (A) Time lapse images show BHK and tsBN2 (BHK with a ts mutation in *RCC1* [Ran GEF]) cells, expressing GFP:anillin (green), treated with Sir-tubulin (red) and Hoechst (stains DNA; blue) during cytokinesis at permissive (33°C) and restrictive temperatures (39.7°C). The scale bar is 10 μm . A bar graph shows the proportions of cytokinesis phenotypes observed for the different cell types and conditions. The data were analyzed using Fisher's exact test (* $p < 0.05$; ** $p < 0.01$) and the n 's are indicated on the graph. (B) Schematic shows how cortical anillin accumulation was measured. Line graph shows a cortical line scan of anillin:GFP around the cell perimeter, with the length (pixels) on the X axis and fluorescence intensity (a.u.) on the Y axis. Regions of the cortex with anillin above 50% maximum levels were summed together to generate the total breadth of accumulated anillin. Dot plot shows the ratio of accumulated anillin to cell perimeter for tsBN2 cells at permissive ($n = 9$) or restrictive ($n = 16$) temperature. The means are indicated, and the data were analyzed using Student's t test (** $p < 0.01$).

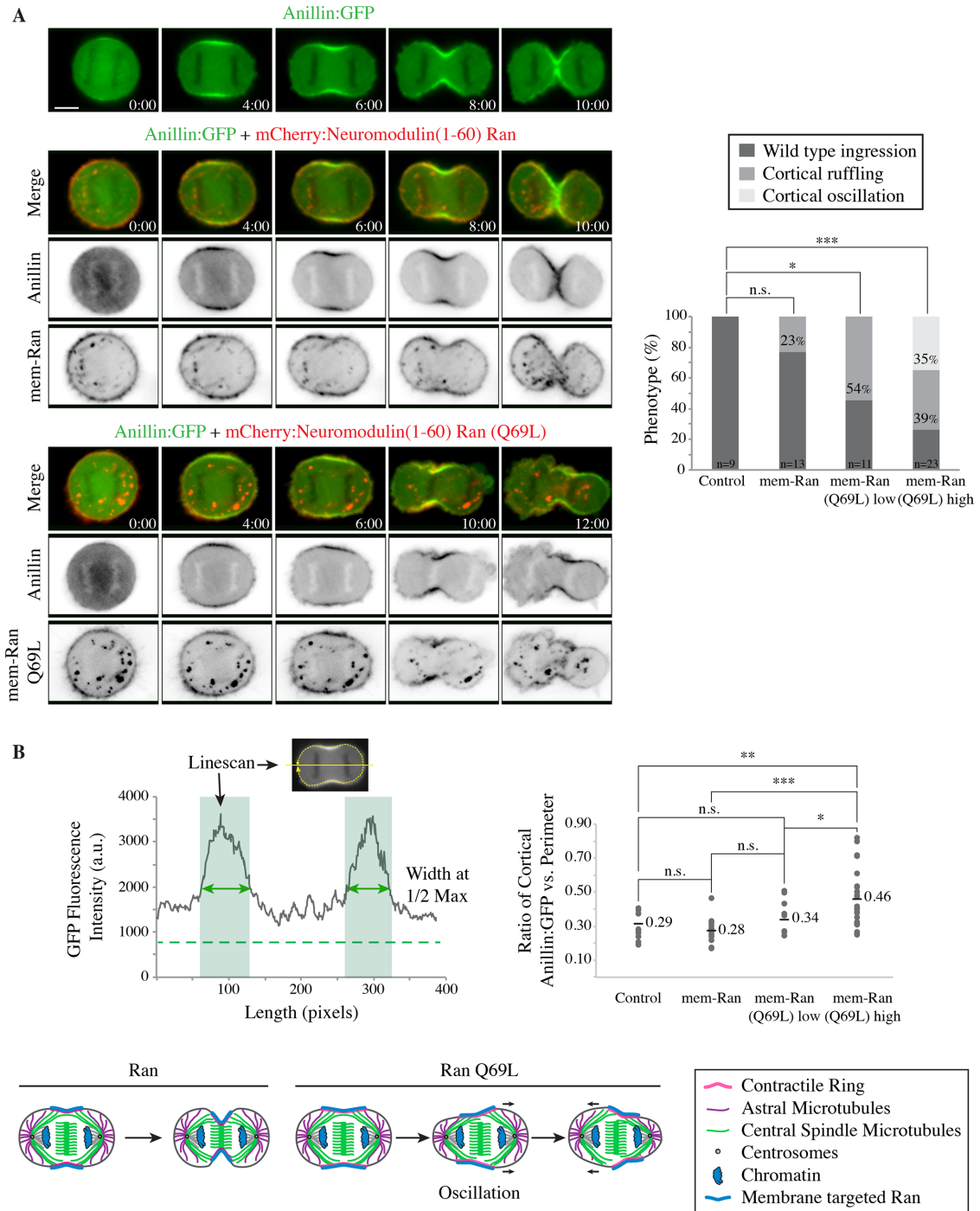


FIGURE 2: Furrow-localized active Ran causes cytokinesis phenotypes. (A) Time lapse images show HeLa cells expressing anillin:GFP (green; top panel), or coexpressing anillin:GFP and mCherry:Ran (mem-Ran; red; 1500–3000 a.u.; middle panels) or RanQ69L (mem-Ran[Q69L]; 1500–3000 a.u.; bottom panels) fused to the phospholipid-binding domain of neuromodulin (1–60) during cytokinesis. The scale bar is 10 μ m. To the right, a bar graph shows the proportions of cytokinesis phenotypes observed in the different cells, as indicated. Cells coexpressing anillin:GFP and low levels of mem-RanQ69L (460–1500 a.u.) were also included in the analysis. The data were analyzed using Fisher's exact test (n.s., not significant, $*p < 0.05$, $***p < 0.001$) and the n 's are indicated on the graph. (B) Line graph shows a cortical line scan of anillin:GFP around the cell perimeter, with the length (pixels) on the X axis and fluorescence intensity (a.u.) on the Y axis. The width of the peak at 50% maximal levels of intensity represents breadth. Dot plot shows changes in the ratio of the breadth of anillin to cell perimeter for control ($n = 9$), membrane-targeted Ran ($n = 13$), low-expressing membrane-targeted Ran(Q69L; $n = 11$) and membrane-targeted Ran(Q69L; $n = 23$). The means are indicated, and p values were determined by Student's t test (n.s., not significant, $*p < 0.05$, $**p < 0.01$, $***p < 0.001$). At the bottom, cartoon schematics show the oscillation phenotype observed in cells overexpressing membrane-targeted Ran (Q69L). The components of the cell are shown in the legend.

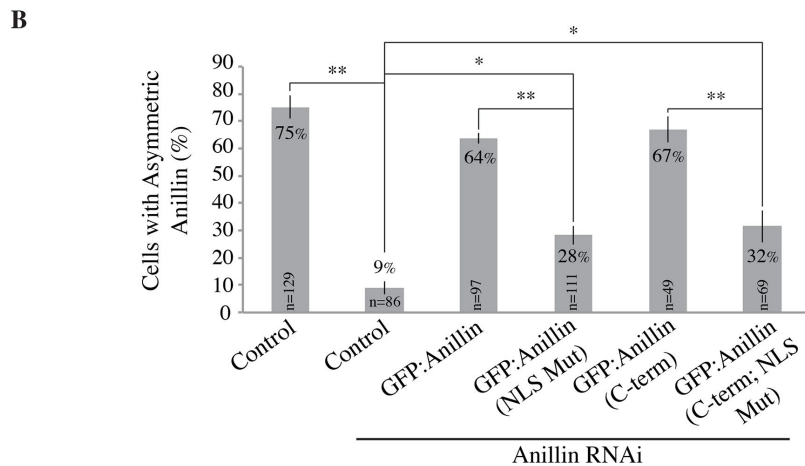
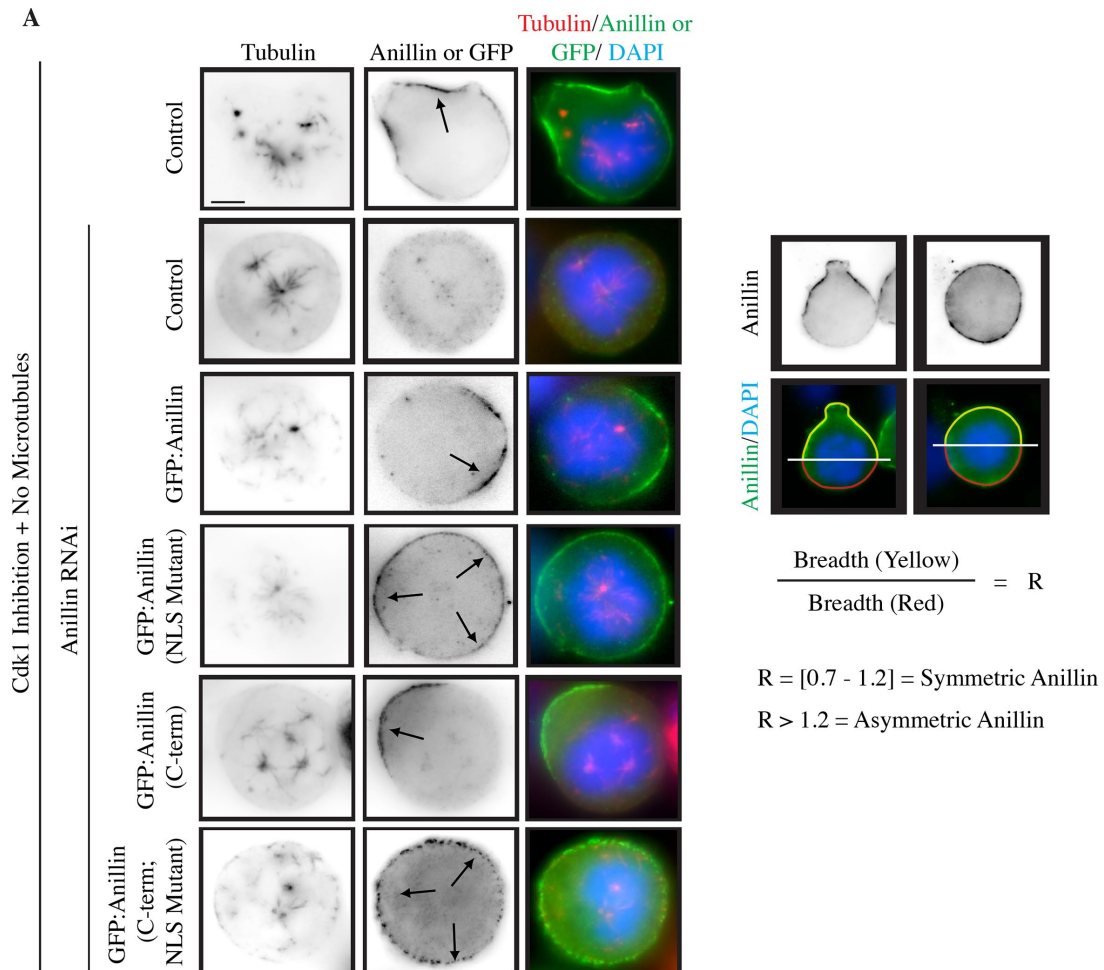


FIGURE 3: Anillin is required for cortical polarity in the absence of polymerized microtubules. (A) Images show fixed HeLa cells treated with anillin RNAi and coexpressing RNAi-resistant full-length GFP:anillin, (1–1087) or C-terminal GFP:anillin (608–1087; C-term) with or without mutations in the C-terminal NLS (850 KK 851- DE; NLS Mutant), treated with 100 nM nocodazole and 22.5 μM Purvalanol A to depolymerize microtubules and induce mitotic exit, respectively. Cells were costained for endogenous anillin or GFP (green), tubulin (red), and DAPI (chromatin; blue). Black arrows indicate regions of the cortex where anillin accumulates. The scale bar is 10 μm . To the right is a schematic to show how anillin's cortical localization was determined to be asymmetric. In cells where the cortex was polarized, a line was drawn through chromatin, perpendicular to the axis of polarization. Line scans were drawn around the cortex in each region (e.g., red vs. yellow) to measure the accumulation of anillin. In cells where the cortex was round, a line was drawn arbitrarily through chromatin, and each side was measured. The ratio R of accumulated anillin was determined, and $R > 1.2$ was defined as asymmetric. (B) Bar graph shows the percentage of cells with asymmetric anillin distribution after rescue with the different anillin constructs as indicated. Bars show SD, and p values were determined by Student's t test ($*p < 0.05$, $**p < 0.01$). The n 's are indicated on the graph.

with septin(s) at the nearby cortex (Silverman-Gavrila *et al.*, 2008). However, it is not clear how this model fits with other published data showing that Ran-GTP inhibits rather than promotes anillin's cortical localization during mitotic exit (Kiyomitsu and Cheeseman, 2013). Our data are consistent with the hypothesis that Ran-GTP negatively regulates anillin's cortical localization. However, in addition to using *Drosophila* rather than mammalian cells, different methods were used (gain-of-function vs. loss-of-function), and the model could be more complex than either study revealed.

The NLS in human anillin maps to a disordered loop emanating from the C2 domain at the C-terminus (Sun *et al.*, 2015). To determine if the C-terminal NLS in human anillin is functional, we expressed different GFP-tagged anillin constructs and monitored nuclear localization in interphase HeLa cells (Figure 4A). Nuclear localization was determined to be positive if the ratio of GFP in the nucleus to that in the cytosol was >1.3, and only cells with levels >1200 a.u. were considered (see Supplemental Figure S3A). The full length and the N-terminus of anillin (1–460) were previously reported to localize to the nucleus in interphase cells (e.g., Figure 4A; Oegema *et al.*, 2000; Chen *et al.*, 2015). The C-terminus (608–1087; RhoA-GTP binding domain – RBD + C2 + Pleckstrin homology domain – PH) and a fragment containing the N-terminal actin and myosin domains and the C-terminal PH domain are nonnuclear (e.g., Figure 4A; Piekny and Glotzer, 2008; Chen *et al.*, 2015). We found that a fragment lacking the RBD (748–1087; C2 + PH) was nuclear (Figure 4A). The localization of C-terminal fragments to the nucleus had been reported previously, but it was not clear why some fragments localized more strongly than others (Oegema *et al.*, 2000). We propose that the C-terminal NLS is inhibited intramolecularly by the RBD during interphase. Treating cells with 100 nM Importazole for 8 h decreased nuclear localization of the C2 + PH fragment, while point mutations in the NLS (850 KK 851- DE) blocked nuclear localization altogether (Figure 4A). Higher concentrations of Importazole were not used, because they affected cell viability. These data suggest that the C-terminal NLS of anillin is responsive to the Ran pathway for nuclear import.

We further assessed whether the C-terminal NLS could respond to Ran via binding to importins. This site matches the consensus sequence of a classic bipartite NLS, which binds to importin- β to mediate nuclear entry, and is highly conserved among vertebrates (Figure 4B; Soniat and Chook, 2015). As mentioned above, the C-terminal NLS also appears to be conserved in *Drosophila*, where it has been shown to bind to importins. However, it is not clear whether this conservation extends to *Caenorhabditis elegans*, as the sequence is more divergent. We pulled down Myc-tagged importin- β from cell lysates using recombinant MBP-tagged human anillin constructs that contained or lacked the RBD (Supplemental Figure S3, B and C, and Figure 4B). As expected, Myc:importin- β localized to the periphery of the nucleus and cytosol in HeLa cells (Supplemental Figure S3B). Myc:importin- β bound weakly to an anillin fragment containing the RBD, but bound more strongly to a fragment lacking the RBD, and mutations in the C-terminal NLS (850 KK 851- DE) abolished binding altogether (Supplemental Figure S3C and Figure 4B). These mutations did not impart gross structural changes in the C-terminus of anillin, because Ect2 and RhoA binding were not affected (Supplemental Figure S3D; Piekny and Glotzer, 2008; Frenette *et al.*, 2012).

The C-terminal NLS of anillin regulates polarization and cytokinesis

Next, we determined the function of anillin's C-terminal NLS in cortical polarity. To do this, rescue assays were performed expressing GFP-tagged RNAi-resistant full-length or C-terminal anillin con-

structs with the NLS point mutations described above (850 KK 851- DE; NLS mutant) in anillin-depleted cells lacking polymerized microtubules and forced to exit mitosis (Figure 3A). Cells were assessed 25 min after Cdk1 inhibition, when the majority of control cells had sufficient time to polarize. As described earlier, while the proportion of polarized cells with asymmetric anillin was restored in cells expressing nonmutant anillin constructs (64% for FL and 67% for C-term), cells failed to polarize with NLS mutant anillin (28% for FL and 32% for C-term; Figure 3, A and B). Because Ran-GTP may affect anillin during earlier stages of mitotic exit, we repeated this assay, but examined cells 15 min after Cdk1 inhibition. At this time, the majority of control cells were not polarized, but anillin was cortically recruited (Supplemental Figure S4A). To measure cortical localization, line scans were drawn across the central plane of the cell and the maximum levels of cortical anillin were compared with those in the cytosol (Supplemental Figure S4A). Anillin was considered to be cortical if the ratio of cortical to cytosolic anillin was >1.1 (Supplemental Figure S4A). Indeed, while anillin was recruited cortically in 96% of control cells and in 84% of anillin-depleted cells coexpressing RNAi-resistant GFP:anillin (FL), NLS mutant anillin was cortical in only 29% of the cells (Supplemental Figure S4A). Together, these data suggest that the C-terminal NLS of anillin is needed for cortical recruitment during early stages of polarization, and also to polarize cells in the absence of microtubules. The ability of the mutant constructs to localize cortically during later time points suggests that other proteins and/or lipids are sufficient to recruit anillin to the cortex.

Next, we determined whether the C-terminal NLS of anillin is required for cytokinesis. GFP-tagged RNAi-resistant FL or NLS mutant anillin was expressed in anillin-depleted cells coexpressing H2B:mRuby to visualize chromatin, and cells were imaged during cytokinesis (Figure 5A). Anillin accumulated along the equatorial cortex ~2 min after anaphase onset, which narrowed as the contractile ring ingressed to pinch in the cell (Figure 5, A and B). However, mutant anillin was recruited to a narrow region ~6 min after anaphase onset, and cytokinesis failed in a larger number of cells (33% vs. 12% for control cells; Figure 5, A and B). Interestingly, although this delay in accumulation correlated with an overall delay in ingression, once mutant anillin was recruited, the time from accumulation to ingression did not vary in comparison with that in nonmutant anillin (Figure 5B). To further test the need for the C-terminal NLS in cytokinesis, we also performed rescue assays in asynchronous populations of cells and calculated the proportion of cells that were binucleate and failed cytokinesis. Anillin depletion caused cytokinesis failure (63% vs. 6% untreated cells; Figure 5B), while expression of RNAi-resistant full-length anillin restored cytokinesis in the majority of cells, consistent with previous studies (24%; Figure 5B; Piekny and Glotzer, 2008). However, a higher proportion of cells expressing RNAi-resistant NLS mutant anillin failed cytokinesis (41%; Figure 5B), supporting the conclusion that the C-terminal NLS is at least partially required for cytokinesis.

To further characterize the effect of the NLS mutations on anillin localization, changes in the breadth of nonmutant versus mutant anillin were quantified by measuring the ratio of cortical anillin to cell perimeter. Mutant anillin was narrower than nonmutant anillin (Figure 5B), although the peak of intensity was comparable (unpublished data). A C-terminal anillin construct containing the NLS mutations also appeared to localize with a narrower breadth than in nonmutant anillin (unpublished data). Collectively, these data suggest that the C-terminal NLS is needed to mediate anillin's recruitment and distribution at the equatorial cortex during anaphase for optimal contractile ring ingression. To show that pools of importin- β localize to the equatorial cortex, line scans were drawn across the

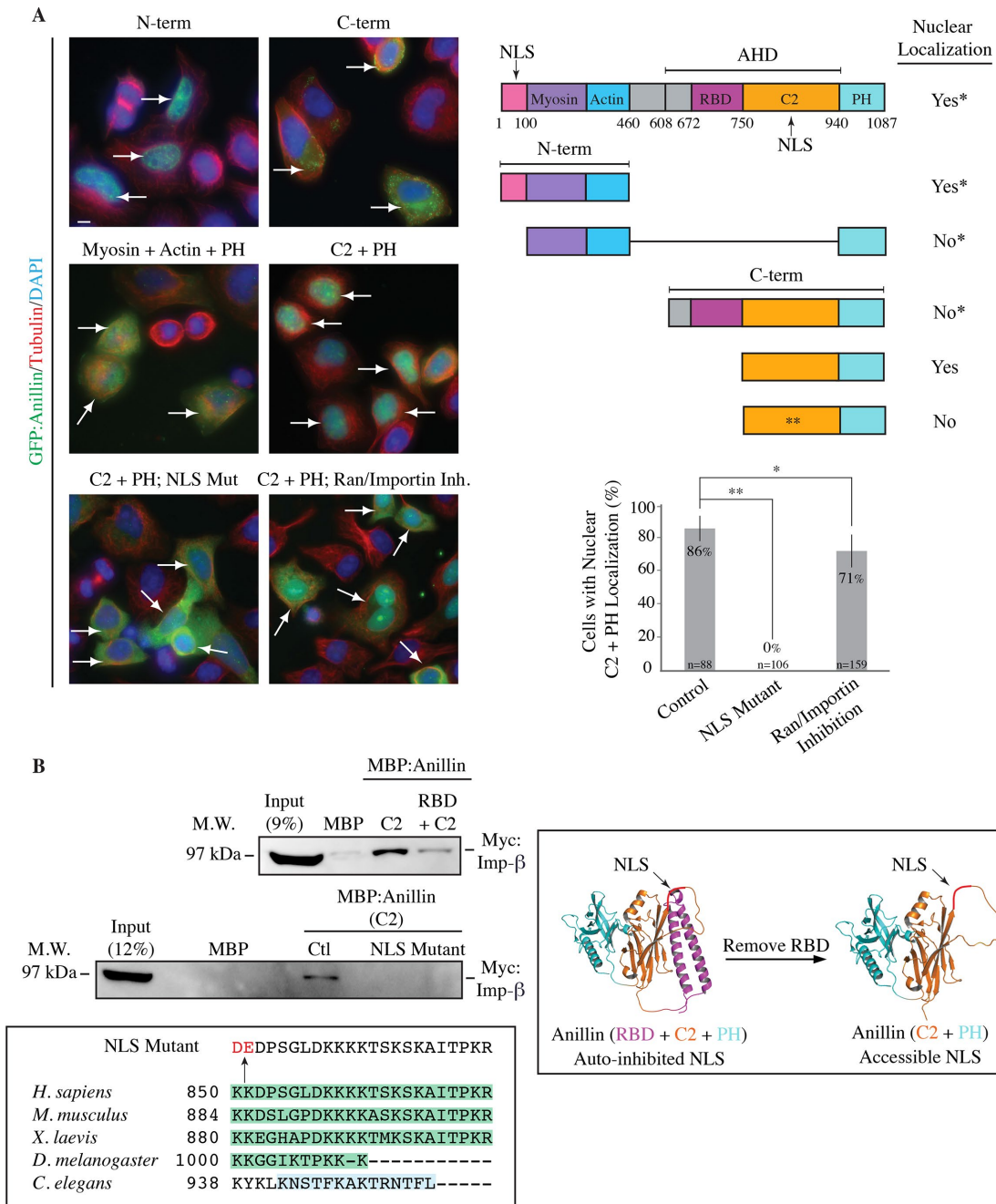


FIGURE 4: Anillin contains a functional NLS in its C-terminus. (A) Images show fixed HeLa cells expressing GFP:anillin constructs costained for GFP (green), tubulin (red), and DAPI (chromatin; blue). White arrows indicate cells with expression levels above 1200. The scale bar is 10 μ m. To the right, a schematic shows the structure of anillin, with its binding domains in different colors (myosin, purple; actin, blue; RBD, dark pink; C2, orange; PH, cyan) and corresponding amino acid numbers, as well as the locations of the N-terminal and C-terminal NLSs, and point mutations within the C-terminal NLS as indicated (**). The AHD (anillin homology domain) is also shown. Constructs that localize to the nucleus are indicated as “yes” or “no” based on previous studies (e.g., Oegema *et al.*, 2000; Piekny and Glotzer, 2008; Chen *et al.*, 2015), or this study. Underneath, a bar graph shows the percentage of cells with nuclear anillin (C2 + PH). Bars show SD, and *p* values were determined by Student’s *t* test (**p* < 0.05, ***p* < 0.01). The *n*’s are indicated on the graph. (B) Immunoblots show pull downs of Myc:importin- β from lysates with purified MBP and MBP-tagged anillin proteins as indicated (C2 vs. RBD + C2 and C2 vs. C2 NLS mutant). An alignment of the C-terminal NLS is shown for human (*Homo sapiens*) anillin with mouse (*Mus musculus*), frog (*Xenopus laevis*), *Drosophila* (*D. melanogaster*), and *C. elegans*. Sequences highlighted in green are strongly predicted to be NLSs, or have been shown to bind to importins (Silverman-Gavrila *et al.*, 2008), while the amino acids highlighted in blue are weakly predicted to be NLSs. The box to the right shows structures for the RBD, C2, and PH (modified from Sun *et al.*, 2015) to demonstrate how the NLS in the C2 domain of anillin may be intramolecularly inhibited by the RBD.

equatorial plane, and Myc:importin- β levels were compared with those of endogenous anillin (Figure 5C). Indeed, the two proteins overlapped at cortical peaks in the equatorial plane (Figure 5C). However, we were surprised to see that the overexpression of Myc:importin- β (levels 1500–4000 a.u.) decreased the breadth of endogenous anillin (Figure 5C). As described earlier, a previous study found that there was competition between importin- α and a putative septin binding site in the C-terminus of *Drosophila* anillin (Silverman-Gavrila *et al.*, 2008). Therefore, high levels of importin- β could similarly hinder the binding of proteins and/or lipids to the C-terminus of human anillin. Together, our data suggest that free importins (e.g., not bound to Ran-GTP) may function as a molecular ruler for anillin, where optimal levels facilitate recruitment, as opposed to when levels are too low or high.

The timing of Ran-regulation of anillin likely occurs during anaphase, prior to furrow ingression. During this time, sister chromatids move toward the poles, where Ran-GTP levels influence anillin's cortical recruitment and localization in the equatorial plane via importins. To further test this model, we compared the temporal and spatial accumulation of nonmutant and mutant anillin in relation to chromatin position. As with the experiments above, cells were depleted of endogenous anillin and rescued with GFP-tagged RNAi-resistant nonmutant versus mutant anillin. An ImageJ (National Institutes of Health) macro was written to sample the intensity of anillin (in a circular region of interest [ROI] 320 nm in radius) at 43 evenly spaced points around the cortex, as well as the distance from these points to the closest point of a mask describing chromatin (see cartoon, Figure 6A). Measurements were taken every 2 min from anaphase onset until 6 min after, and the data from five cells for nonmutant versus mutant anillin were averaged and graphed (Figure 6A). Consistent with our model, the accumulation and clearance of cortical nonmutant anillin strongly correlated with changes in chromatin distance (Figure 6A). However, there was no correlation with mutant anillin until 6 min after anaphase onset, when the central spindle likely promotes the accumulation of active RhoA and anillin in the equatorial plane (van Oostende Triplet *et al.*, 2014). These data suggest that the localization of mutant anillin likely is not influenced by chromatin or Ran-GTP.

Importin binding influences anillin's affinity for the equatorial cortex

Our analyses of NLS mutant anillin suggest that disrupting importin binding weakens anillin's affinity for the equatorial cortex. Typically, the boundary of equatorial anillin tightly matches active RhoA, and will loosely correlate with mitotic spindle position (yellow arrows; Figure 6B; Piekny and Glotzer, 2008; van Oostende Triplet *et al.*, 2014). The decrease in breadth of mutant anillin's localization is similar to what we observed when the proportion of astral microtubules was increased near the equatorial plane via MCAK RNAi (Zanin *et al.*, 2013; van Oostende Triplet *et al.*, 2014). Indeed, the localization of NLS mutant anillin tightly matched the boundary of microtubules near the equatorial cortex (white arrows), while nonmutant anillin loosely correlated with their position as shown previously (Figure 6B; van Oostende Triplet *et al.*, 2014). We previously reported that the C-terminus of anillin bound weakly to microtubules *in vitro* (Tse *et al.*, 2011; van Oostende Triplet *et al.*, 2014). Because importin- β binding to the C2 domain is inhibited by the RBD, we compared microtubule binding to the C-terminus and the C2 domain using cosedimentation assays. Microtubules bound more strongly to the C2 domain than to the C-terminus (Figure 6C). In addition, a deletion that removes the NLS and a small region upstream (DFEINIE) that lies at the hinge of the RBD and C2 also

bound to microtubules more strongly (unpublished data; Piekny and Glotzer, 2008). Therefore, the microtubule-binding domain is auto-inhibited by the RBD, similarly to the NLS. We did not observe a significant change in microtubule binding with the C2 NLS mutant (Supplemental Figure S4B). Thus, the change in NLS mutant anillin localization in cells suggests that there is a reduction in its affinity for the equatorial cortex.

To further show that the localization of NLS mutant anillin at the equatorial plane is strongly regulated by microtubules, we monitored changes in its localization after depolymerizing astral microtubules using a low dose of nocodazole (33 nM). The localization of nonmutant and mutant anillin broadened along the equatorial cortex to a similar extent, supporting the conclusion that microtubules were responsible for restricting mutant anillin localization (Figure 5, A and B). We previously reported that both the central spindle and astral microtubules contribute to restricting anillin localization, and this is why we do not see anillin expanding into the polar regions of the cell (van Oostende Triplet *et al.*, 2014).

DISCUSSION

Our studies shed light on a microtubule-independent mechanism that ensures robust cytokinesis. Previous studies showed that HeLa cells lacking polymerized microtubules polarize, and the contractile protein anillin localizes away from chromatin (Kiyomitsu and Cheeseman, 2013). Ran-GTP is required for this polarization, because anillin fails to move away from chromatin after reducing the activity of its GEF, RCC1, or reducing Ran-GTP-importin binding using the drug Importazole (Supplemental Figure S2B; Kiyomitsu and Cheeseman, 2013). Thus, a Ran-GTP gradient associated with chromatin may lead to relaxation of the polar cortex when the mitotic spindle shifts too close to one pole to restore the cleavage plane (Kiyomitsu and Cheeseman, 2013). Our studies add to this model by showing that anillin is a molecular target of the Ran pathway during cytokinesis. Anillin is a key regulator of cytokinesis that binds to multiple contractile ring components including RhoA, and we have shown that anillin can feed back to influence active RhoA *in vivo* (Piekny and Glotzer, 2008; Frenette *et al.*, 2012). We propose that the Ran pathway modulates cytokinesis by affecting anillin's recruitment to the cortex. During mitotic exit, RhoA-GTP levels increase and bind to the RBD of anillin, causing a change in its conformation that makes other binding sites in the C-terminus more accessible, including the NLS and microtubule-binding domain. Importin binding may stabilize this open conformation to further enhance anillin's recruitment to the cortex. However, in the vicinity of chromatin, high Ran-GTP would bind to importin(s) and prevent it from binding to, or promote its release from cargo such as anillin, which would favor anillin's cytosolic localization. Free importins (e.g., not bound to Ran-GTP, but possibly bound to cargo) form an inverse gradient to Ran-GTP, with optimal levels likely occurring near the cortex, where importin- β could bind to anillin and favor its cortical recruitment (Figure 6D).

We have several pieces of evidence to support our model. First, we show that Ran-GTP levels influence the localization of contractile proteins and cause cytokinesis phenotypes. Reducing the levels of Ran-GTP led to the ectopic recruitment of anillin and myosin to regions of the cortex where they normally would not accumulate, likely causing a change in cortical properties at the cell poles and blocking furrow ingression (Figure 1). Consistent with a function for Ran-GTP in negatively regulating anillin, increasing the levels of active Ran in the equatorial furrow caused a reduction in anillin and cortical instability phenotypes similar to anillin loss-of-function (Figure 2). There are two ways that Ran-GTP could do this: 1) by directly binding to and competing with importins from cargo/target

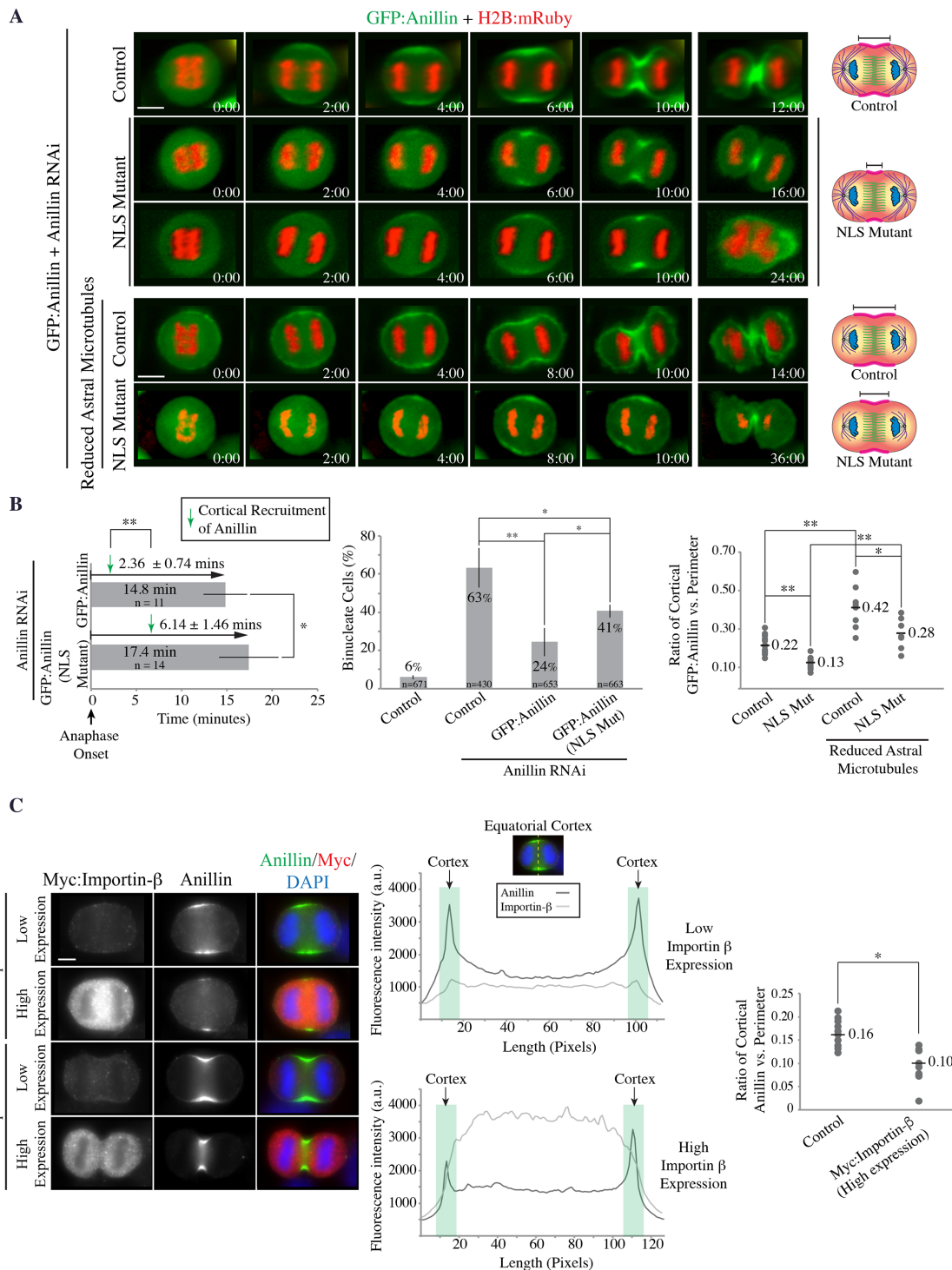


FIGURE 5: The C-terminal NLS regulates anillin's function during cytokinesis. (A) Time lapse images show HeLa cells depleted of anillin, expressing GFP-tagged RNAi-resistant nonmutant ($n = 17$) or NLS mutant anillin ($n = 21$) coexpressing H2B:mRuby. Also shown are cells after treatment with 33 nM nocodazole to reduce astral microtubules ($n = 7$ for nonmutant and $n = 7$ for mutant anillin). Cartoon cells to the right show changes in the distribution of anillin under the different conditions. The scale bar is 10 μm . (B) Bar graph shows a comparison of the timing of anillin recruitment (green arrow) and time from anaphase onset to complete furrow ingression for anillin-depleted cells rescued with nonmutant anillin in comparison with NLS mutant anillin from anaphase onset. Standard deviations are shown as bars and as times for cortical recruitment, and the data were analyzed by Student's t test ($*p < 0.05$, $**p < 0.01$). The n 's are shown on the graph. A bar graph in the middle shows the percentage of binucleate cells \pm anillin RNAi and after rescue with GFP-tagged RNAi-resistant nonmutant or NLS mutant anillin. The bars show SD, and p values were determined by Student's t test ($*p < 0.05$, $**p < 0.01$). The n 's are indicated on the graph. The dot plot to the right shows changes in the ratio of the breadth of anillin to cell perimeter in anillin-depleted cells rescued with nonmutant ($n = 15$) or NLS mutant anillin ($n = 21$), and after treatment with nocodazole to reduce astral microtubules ($n = 7$ for

proteins that promote or prevent a specific function, or 2) by regulating nuclear sequestration of cytokinesis regulators. Up-shifting tsBN2 cells to inactivate RCC1 (the GEF for Ran) likely keeps the nuclear envelope from reforming, causing cells to remain in a persistent cytokinesis-like state (Figure 1; Clarke and Zhang, 2008). This may occur because regulators of actomyosin contractility that are normally nuclear in telophase (e.g., Ect2) have continued access to the cortex when the nuclear envelope fails to form. However, our experiment with targeting active Ran directly to the membrane provides evidence that Ran-GTP directly influences the cortex (Figure 2). Second, we found that anillin contains a highly conserved NLS in its C-terminus that binds to importin- β and is required for anillin's localization, cortical polarization, and cytokinesis (Figures 3–6). This site can function in response to the Ran pathway to mediate nuclear entry, but is autoinhibited by the RBD (Figure 4). The RBD also blocks accessibility to anillin's microtubule-binding site (Figure 6). This autoinhibition could ensure that anillin's C-terminus has access to importin or microtubules only when RhoA-GTP levels increase during mitotic exit. A recent study showed that anillin is also regulated by phosphorylation, via a site that lies just N-terminal to the RBD (Kim *et al.*, 2017). An extension of our model is that phosphorylation may further influence RhoA-GTP binding, to couple the timing of changes in anillin's activity with its requirement for cytokinesis. We found that the C-terminal NLS is required for anillin's localization, because the equatorial domain of anillin is more restricted when the NLS is mutated (Figures 5 and 6D). This is similar to what we observed when astral microtubules were enriched in the equatorial plane via MCAK RNAi (van Oostende Triplet *et al.*, 2014), suggesting a decrease in anillin's affinity for the equatorial cortex and a shift toward microtubules in spatially controlling anillin. Indeed, the localization of NLS mutant anillin changes/broadens after astral microtubule perturbation (Figure 5).

Our study reconciled two models that had been proposed to explain how Ran-GTP could influence the cortex (Silverman-Gavrila *et al.*, 2008; Kiyomitsu and Cheeseman, 2013). One study showed that importin- α competes for septin binding in the C-terminus of anillin and could release anillin for septin binding in the vicinity of chromatin during cellularization (Silverman-Gavrila *et al.*, 2008). A different study showed that Ran-GTP inhibited rather than promoted anillin's cortical localization during mitotic exit (Kiyomitsu and Cheeseman, 2013). Our data support the latter model, as described above. However, we also found that overexpression of importin- β decreased the breadth of anillin's localization in the equatorial plane, similarly to the NLS mutant, which cannot bind to importin- β . Thus, we propose a hybrid model where importin binding facilitates anillin's cortical recruitment, but likely binds with low affinity to ensure that anillin can bind favorably to other proteins and lipids. Thus, importins could function as a molecular ruler, whose optimal levels favor the localization of cortical proteins at precise locations as opposed to when they are too high or too low.

A recent study identified a putative phospholipid-binding site in the C2 domain of anillin, which may partially overlap with the C-terminal NLS that we describe here (Sun *et al.*, 2015). It found that

this site functions cooperatively with the RBD to recruit anillin to the cortex (Sun *et al.*, 2015). Our data fit with this previous finding, and importin binding could also influence phospholipid binding, leading to the enhancement of anillin's recruitment to the cortex. It is important to note that the NLS mutations used in this study are not in the predicted phospholipid-binding domain described in Sun *et al.* (2015). Further, although delayed, all of the anillin constructs containing mutations in the NLS localized to the cortex, likely due to their recruitment via other proteins and/or lipids.

The Ran pathway likely regulates the cortex during anaphase. During metaphase, Ran-GTP forms a gradient around chromatin, where it regulates bipolar spindle formation (Kaláb *et al.*, 2002, 2006; Clarke and Zhang, 2008). We propose that Ran-GTP also regulates cortical proteins during mitotic exit. We observed a strong correlation of the timing and spatial distribution of anillin's cortical localization with the distance of the segregating sister chromatids (Figure 6). This correlation was no longer apparent when the NLS was mutated, which was only recruited to a narrow region of the furrow ~6 min after anaphase onset, likely via the central spindle (Figure 6). The regulation of protein–protein interactions via importins is not a new concept, but our model expands the understanding of how importins could regulate the conformation and function of cortical proteins. While our studies were performed in HeLa cells, which divide symmetrically, it would be interesting to determine if the Ran-anillin pathway more dominantly regulates cytokinesis in asymmetrically dividing cells. Furthermore, this pathway may improve the robustness of cytokinesis in cancer cells with high chromosomal instability and altered ploidy, particularly because cancer cells with polyploidy have steeper Ran-GTP gradients (Hasegawa *et al.*, 2013).

MATERIALS AND METHODS

Cell culture, transfection, and drug treatments

HeLa, BHK, and tsBN2 (with a ts mutation in RCC1 in BHK) cells were plated and grown in DMEM (Wisent), supplemented with 10% fetal bovine serum (FBS; Thermo Scientific), 2 mM L-glutamine (Wisent), 100 U penicillin, and 0.1 mg/ml streptomycin (Wisent) with 5% CO₂. HeLa cells were maintained at 37°C, and BHK and tsBN2 cells were maintained at 33°C. For transfection, cells were plated in DMEM media without antibiotics (PS) and transfected using Lipofectamine 2000 (DNA or DNA and siRNA cotransfection in HeLa, BHK, or tsBN2 cells; Invitrogen) or Oligofectamine (siRNA transfection in HeLa cells; Invitrogen) according to the manufacturer's protocol, except that 4 μ l of Lipofectamine was used per 2 ml of media with 0.5–1.5 μ g DNA and 3 μ l of 2 nM siRNAs, as described previously (Yüce *et al.*, 2005; Piekny and Glotzer, 2008). Cells were imaged 24–26 h after DNA transfection, and 27–30 h after cotransfection of DNA and siRNAs.

Anillin and Ect2 siRNAs were used as described previously (Yüce *et al.*, 2005; Piekny and Glotzer, 2008). The following drugs were used and dissolved in dimethyl sulfoxide (DMSO; Sigma-Aldrich) as 1000X stocks: Importazole (Sigma-Aldrich), S-trityl-L-cysteine (STC; Sigma-Aldrich), Blebbistatin (Sigma-Aldrich), and Purvalanol A

wild type and $n = 7$ for NLS mutant). The means are indicated, and the data were analyzed by Student's t test ($*p < 0.05$, $**p < 0.01$). (C) Images show fixed cells expressing Myc:importin- β (red), costained for anillin (green) and DAPI (blue) in anaphase or during furrow ingression (telophase) as indicated. Line scans show the levels of anillin vs. Myc across the equatorial plane (dotted yellow line) in a cell with low levels of Myc (<1000 a.u.; top) or high levels of Myc (1500–4000 a.u.; bottom), with length (pixels) on the X axis and fluorescence intensity (a.u.; dark gray = anillin, light gray = importin- β) on the Y axis. The green rectangles highlight regions of the equatorial cortex. To the right is a dot plot of the ratio of the breadth of anillin to the perimeter in cells with low (control, $n = 11$) vs. high Myc ($n = 9$). The data were analyzed by Student's t test ($*p < 0.05$).

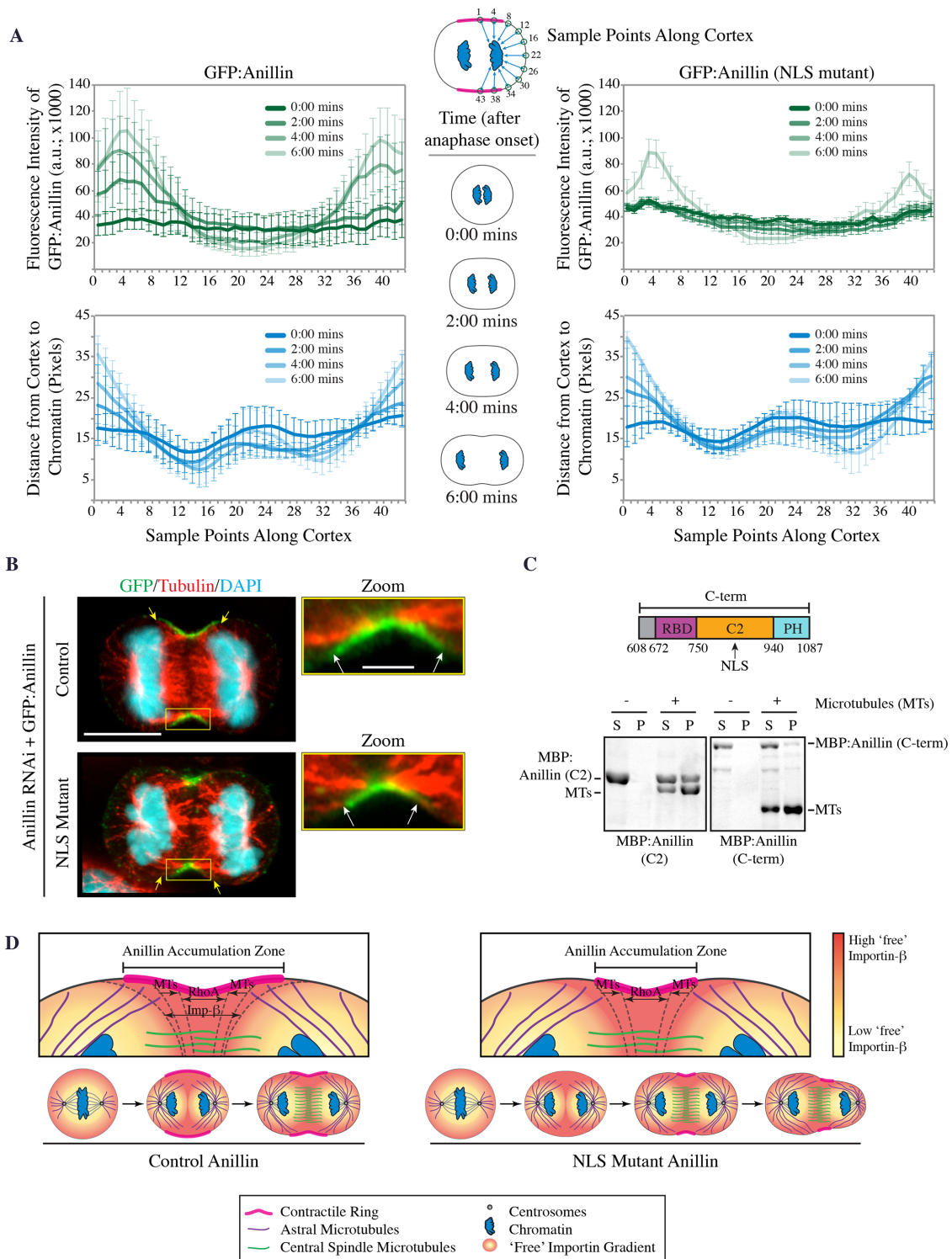


FIGURE 6: The C-terminal NLS influences anillin's affinity for the equatorial cortex during cytokinesis. (A) A macro written for ImageJ measured average anillin intensity at 43 points around the cortex as well as the distance from each point to chromatin. Line graphs show anillin intensity (top graphs; green) and distance to chromatin (bottom graphs; blue) as indicated in the schematic at the top, from anaphase onset to early ingress. The graphs on the left show measurements from anillin-depleted cells rescued with GFP-tagged RNAi resistant anillin ($n = 5$ cells), and the graphs on the right show anillin-depleted cells rescued with GFP-tagged RNAi resistant NLS mutant anillin ($n = 5$ cells). Bars show SD. (B) Images show HeLa cells treated with anillin RNAi expressing GFP-tagged RNAi-resistant anillin or NLS mutant anillin, costained for GFP (green), tubulin (red), and DAPI (chromatin; cyan). Yellow arrows point to astral microtubules. The scale bar is 10 μm . Zoomed-in regions in the boxed insets show anillin and microtubules at the furrow, as indicated. White arrows point to the demarcation of anillin localization. The scale bar is 2 μm . (C) Cartoon schematic shows binding domains in the C-terminus of anillin (RBD, C2, PH). Below are Coomassie-stained gels of cosedimentation assays

(Sigma-Aldrich). To make cells monopolar, 2 μM of STC was used to arrest cells in prometaphase, followed by the addition of 22.5 μM Purvalanol A to promote mitotic exit (Hu *et al.*, 2008). For nocodazole (Sigma-Aldrich) treatments, 33 nM was added to cells 3 min after anaphase onset to selectively disrupt astral microtubules, while 100 nM was added to cells for 3–4 h to depolymerize the majority of microtubules and cause mitotic arrest. A dose of 22.5 μM Purvalanol A was then added to promote mitotic exit during imaging. A dose of 100 μM Blebbistatin was added to cells to inhibit myosin II activity during imaging. A dose of 100 nM Importazole was added to HeLa cells either for 4 h in combination with nocodazole to test for changes in polarization, or for 8 h to test for changes in the nuclear localization of anillin. Control cells were treated with DMSO for all of the experiments involving drug treatments.

tsBN2 cells with a ts mutation in RCC1 were generously provided by I. Cheeseman (Whitehead, MIT; Nishimoto *et al.*, 1978; Kiyomitsu and Cheeseman, 2013). HeLa cells stably expressing GFP:nonmuscle regulatory myosin light chain (T18E S19E) and anillin:GFP have been described previously (Zanin *et al.*, 2013; van Oostende Triplet *et al.*, 2014). Myc-tagged human karyopherin (importin- β 1; KPNB1; accession number NM_002265) cDNA was obtained from Origene.

H2B:mRuby was generated from H2B:GFP, generously provided by G. Hickson (University of Montreal). GFP was replaced with mRuby using *Bam*HI (New England Biolabs) and *Xba*I restriction enzymes (New England Biolabs) and pcDNA3-mRuby2 plasmids kindly provided by C. Brett (Concordia University). mCherry:neuromodulin (1–60) Ran (WT) was generated via PCR using Ran cDNA (True Clone), and the pTK24 plasmid (Addgene) using *Xho*I and *Eco*RI restriction enzymes (New England Biolabs). Ran Q69L was generated in the same vector by PCR-based site-directed mutagenesis. GFP:Ran and GFP:Ran (Q69L) was cloned into pEGFP-C1 (Life Technologies) using *Xho*I and *Eco*RI restriction enzymes. The anillin constructs were previously described (Piekny and Glotzer, 2008), except for GFP:anillin (748–1087), which was cloned into pEGFP-C1 (Life Technologies) using *Hind*III and *Sac*I restriction enzymes. mRuby:anillin was generated from GFP:anillin by replacing GFP with mRuby using *Age*I and *Sac*I restriction enzymes. The 850 KK 851-DE mutations were generated in the anillin constructs by PCR-based site-directed mutagenesis. All constructs were verified by sequencing.

Fixation, immunofluorescence, and live imaging

Cells were fixed for immunofluorescence using 10% trichloroacetic acid (TCA) or 100% cold methanol as previously described (Yüce *et al.*, 2005). Fixed cells were immunostained for microtubules using 1:200 mouse anti-tubulin antibodies (DM1A; Sigma-Aldrich), anillin using 1:200 rabbit polyclonal anti-anillin antibodies (Piekny and Glotzer, 2008), GFP using 1:100 mouse Clones 7.1 and 13.1 (Roche) or 1:200 rabbit anti-GFP polyclonal antibodies generously provided by M. Glotzer (University of Chicago). Anti-rabbit or mouse Alexa 488 and anti-mouse or rabbit Alexa 568 (Invitrogen) secondary antibodies were used at a 1:250 dilution. 4',6-Diamidino-2'-phenylindole dihydrochloride (DAPI; Sigma-Aldrich) was added at a 1:1000 dilution (1 mg/ml stock) for 5 min before the coverslips were mounted onto slides. Fixed cells were imaged using a Fluoview FV10i confocal laser

scanning microscope (Olympus) with a 60 \times /1.35 oil immersion objective and 3 \times magnification (total magnification 180 \times). Images were acquired as 0.5- μm Z-stacks with the pinhole set at 1 Airy unit. Fixed cells also were imaged using a Leica DMI6000B wide-field microscope with a 63 \times /1.4 PL APO oil immersion objective (pixel size 0.102 μm), and Z-stacks of 0.5 μm were acquired with a Hamamatsu OrcaR2 camera and Volocity software (PerkinElmer) using a piezo Z stage (MadCityLabs). Fixed cells also were imaged at high resolution using the Zeiss LSM800 Airyscan mode with a C-APO 63 \times /1.2 oil immersion objective, and Z-stacks of 0.17 μm using a 32 channel GaAsP Airyscan spatial detector that provides spatial resolution 1.7 \times , typically achieved via confocal imaging at 1 Airy unit. Image files were exported as TIFFs, which were opened with ImageJ and converted into maximum-intensity Z-stack projections. Projections and merged color images were then converted into 8-bit images and imported into Illustrator (Adobe) to make figures.

To perform live imaging, media was replaced with phenol red-free DMEM. Cells were plated and transfected on 25-mm round coverslips (No. 1.5) placed in a 35-mm Chamlide magnetic chamber (Quorum), or on a 35-mm μ -dish with volume 2 ml (ibidi), or on μ -slide angiogenesis tissue culture-treated 15-well dishes (ibidi). Cells were kept at 37°C (except for BHK and tsBN2 cells, which were kept at either 33 or 39.7°C) with 5% CO₂ using the INU-TiZ-F1 chamber (MadCityLabs). For BHK and tsBN2 cells, Sir-tubulin (Cytoskeleton) was added to a final concentration of 200 nM 3–4 h before filming, and Hoechst 33342 (Invitrogen) was added to a final concentration of 160 nM 30–40 min before filming. tsBN2 cells were up-shifted for 30–40 min before imaging. Live imaging was performed on an inverted Nikon Eclipse Ti microscope with a Livescan Swept Field confocal unit (Nikon), using a 60 \times /1.4 CFI PLAN APO VC oil immersion objective (pixel size 0.27 μm), a piezo Z stage (MadCityLabs), and an iXON897 EMCCD camera (Andor). Images were acquired with 200 ms exposures using 488- and 561-nm lasers (100 mW, Agilent) set between 20 and 40% power, depending on the intensity of fluorescence signals (settings were kept constant for related experiments), and multiple Z-stacks of 0.5 μm were taken every 40–60 s per cell using NIS-Elements acquisition software (Nikon) and a narrow GFP or dual filter (500–544 and 600–665 nm; Chroma). The tsBN2 cells were kept at 33°C (permissive temperature) and were up-shifted to the restrictive temperature (39.7°C) to inactivate RCC1 in late metaphase or immediately following anaphase onset. All of the images coexpressing GFP and mRuby or mCherry probes were spectrally unmixed using the NIS-Elements acquisition software (Nikon) and deconvolved using Autoquant X software (Media Cybernetics). Image files were exported as TIFFs, which were opened with ImageJ and converted into maximum-intensity Z-stack projections. Projections and merged color images were then converted into 8-bit images and imported into Illustrator (Adobe) to make figures, or saved as AVI movie files.

Pull downs, immunoblots, and cosedimentation assays

Purified protein was made from *E. coli* BL21 cells transformed with the following constructs as described previously (Piekny and Glotzer, 2008): MBP-anillin (C2; 750–872), MBP-anillin (RBD + C2; 672–940),

(S, supernatants; P, pellets) using 1.5 μM purified microtubules (MT) incubated with 1.5 μM purified MBP-tagged anillin proteins as indicated. A comparison between C2 and C-term is shown. (D) Cartoon schematics show anillin vs. NLS mutant anillin (right) localization during anaphase and early telophase. Zoomed-in regions highlight how the zone of anillin is determined by RhoA-GTP and importin- β , the latter of which permits the spread of anillin beyond the boundary of astral microtubules. The levels of free importin- β are determined by the Ran-GTP gradient formed around chromatin.

and MBP:anillin (C-term; 608–1087). NLS mutant MBP-anillin (850 KK 851-DE) was generated in the anillin constructs by PCR-based site-directed mutagenesis. Bacteria were resuspended in lysis buffer (2.5 mM MgCl₂, 50 mM Tris, 150 mM NaCl, pH 7.5, 0.5% Triton X-100, 1 mM dithiothreitol [DTT], 1 mM phenylmethanesulfonyl fluoride [PMSF] and 1X protease inhibitors; Roche), incubated with 1 mg/ml lysozyme on ice for 30 min, and then sonicated three times. Extracts were incubated with amylose resin (New England Biolabs) for 5 h at 4°C with rotation. After being washed, protein loaded beads were stored as a 50% slurry at 4°C or eluted in equivalent volumes of 100 mM maltose on ice for 2 h. Protein concentration was determined before use.

Microtubules were prepared from lyophilized microtubules (Cytoskeleton) per the manufacturer's instructions in resuspension buffer (15 mM PIPES, 1 mM MgCl₂, 20 μM taxol; Bioshop) for 10–15 min at room temperature with gentle mixing. Aliquots of 45.5 μM were flash frozen, stored at –80°C, and then thawed in a circulating water bath and diluted with resuspension buffer to 9.1 μM. Purified anillin proteins were prespun by centrifugation at 279,000 × *g* for 25 min at room temperature. Cosedimentation reactions were prepared as described previously (van Oostende Triplet *et al.*, 2014).

Transfected HeLa cells were lysed in 50 mM Tris, pH 7.6, 150 mM NaCl, 5 mM MgCl₂, 0.5% Triton X-100, 1 mM DTT, and 1 mM PMSF with protease inhibitors (Roche) and incubated with 5–10 μg of purified MBP-tagged anillin protein on amylose resin beads at 4°C to pull down Myc:importin-β, Myc:Ect2 C-terminus (422–881), and GFP:RhoA (Q63L). Beads were washed three to four times with 50 mM Tris, pH 7.6, 150 mM NaCl, and 5 mM MgCl₂ before SDS sample buffer was added to denature the proteins for SDS-PAGE. All pull downs were run by SDS-PAGE and wet-transferred to nitrocellulose membrane for Western blotting. All blots were reversibly stained with Ponceau S to show total protein. Western blots were treated with either mouse anti-Myc antibodies (clone 9E10; DSHB) used directly or 1:2000 mouse anti-GFP antibodies (Roche). The secondary antibody used for all blots was anti-mouse Alexa 488 (Invitrogen). Blots were scanned at 488 nm using the Typhoon Trio phosphoimager (GE). Images were converted to 8-bit by ImageJ and made into figures using Adobe Photoshop and Illustrator (Adobe).

Quantification

The breadths and ratios of cortical accumulation for anillin and myosin were determined using ImageJ. Maximum-intensity Z-projections were generated for each cell, and the breadth was determined using a line scan drawn along the cell cortex. The breadth was determined as the number of pixels above 50% of the maximum intensity (width of the peak) after cytosol levels were subtracted, divided by the total number of pixels to give a ratio of breadth to length of cell perimeter. To measure the ratio of cortical accumulation to cytosol, the average intensity was determined in an area drawn around the cortex from one pole to the other. This value was then divided by the average fluorescence intensity from a ROI from the cytosol. To measure the asymmetric distribution of GFP-tagged anillin, RhoA, and myosin, a line was drawn through chromatin perpendicular to the axis of polarization to bisect the cell. The breadth of accumulation was measured for each half of the cell and a ratio *R* was determined (schematic in Figure 3A). Cells with *R* = [0.7–1.2] were scored as symmetric, while cells with *R* > 1.2 were scored as asymmetric. In cells where there was no visible cortical protrusion, a line was drawn arbitrarily through chromatin. To measure the cortical recruitment of anillin in polarized cells, a

line scan was drawn through the central plane of the cell. The ratio *R* of maximum cortical to maximum cytosolic levels was determined, and anillin was scored as cortical in cells with *R* > 1.1 (schematic in Supplemental Figure S4A). To compare the localization of Myc:importin-β and anillin at the equatorial cortex, a line scan was drawn through the cell at the equatorial axis, and their fluorescence levels were compared in a line graph. To measure the nuclear localization of GFP-tagged anillin, the average fluorescence intensities from ROIs in the nucleus and cytosol were measured and a ratio of nuclear to cytosolic levels *R* was determined. Cells with *R* > 1.3 were scored as nuclear, while cells with *R* < 1.3 were scored as cytosolic. All data were imported into Excel (Microsoft), where calculations were performed, including standard deviations, and graphs were generated. All experiments with fixed cells were replicated at least three times and analyzed using Student's *t* test or one-way analysis of variance. Live imaging experiments were replicated a minimum of five times to obtain sufficient *n*'s, which were pooled and statistically analyzed via Fisher's exact test.

To choose cells with Ran overexpression for analysis in Figure 2, the levels of mCherry-tagged Ran were measured in cells coexpressing GFP-tagged anillin. The exposure time and gain were kept constant for Ran versus Ran Q69L. Cells were determined to have high overexpressed Ran if the levels were above 1500 and below 3000, and to have low expression of Ran if the levels were above 460 and below 1500.

Colocalization measurements between mCherry-tagged Ran and GFP-tagged anillin were performed using the colocalization analysis plug-in in ImageJ. The ROI was determined for each region of the cell cortex (as indicated in Supplemental Figure S1B) after background subtraction, and a scatterplot was generated to show the colocalized pixels with varying intensities for each channel. The percentage of colocalized pixels was determined based on Pearson's coefficient for each cell, and the average for the population was determined. The means of the averages for multiple cells and standard deviations were calculated and graphed in Excel (Microsoft).

The expression levels of the constructs used in Figures 3–6 were determined based on controls. Anillin RNAi cells coexpressing either the full length or the C-terminus of anillin were tested for their ability to polarize and rescue cytokinesis, respectively. The imaging parameters used for the rescued cells were optimized to fluorescence intensities between 1200 and 3500 for the GFP channel and were kept constant for the other constructs to ensure that only cells with sufficient levels of expression were considered.

To assay changes in the localization of GFP-tagged anillin along the cortex during anaphase in relation to chromatin distance, an ImageJ macro was written. Briefly, the cortex of a cell was traced at each time point (anaphase onset; 0, 2, 4, and 6 min), and a series of 43 points (in total) were drawn around each half of the cell, encompassing 220°. At each point, the shortest distance to a binary mask that described the chromatin was measured, and a circular sampling window of diameter 640 nm was used to measure mean anillin intensity.

All of the images and graphs were transferred to Illustrator (Adobe) to make figures.

ACKNOWLEDGMENTS

We thank C. van Oostende Triplet, M. Jaramillo Garcia, and G. Lapointe for help with imaging studies as part of the Centre for Microscopy and Cellular Imaging at Concordia University. We thank C. Brett (Concordia University), I. Cheeseman (Whitehead, MIT), and G. Hickson (University of Montreal) for reagents.

REFERENCES

- Akhshi TK, Wernike D, Piekny A (2014). Microtubules and actin crosstalk in cell migration and division. *Cytoskeleton* 71, 1–23.
- Bement WM, Benink HA, Von Dassow G (2005). A microtubule-dependent zone of active RhoA during cleavage plane specification. *J Cell Biol* 170, 91–101.
- Bringmann H, Hyman AA (2005). A cytokinesis furrow is positioned by two consecutive signals. *Nature* 436, 731–734.
- Cabernard C, Prehoda KE, Doe CQ (2010). A spindle-independent cleavage furrow positioning pathway. *Nature* 467, 91–94.
- Canman JC, Cameron LA, Maddox PS, Straight A, Tirnauer JS, Mitchison TJ, Fang G, Kapoor TM, Salmon ED (2003). Determining the position of the cell division plane. *Nature* 424, 1074–1078.
- Canman JC, Hoffman DB, Salmon ED (2000). The role of the pre- and post-anaphase microtubules in the cytokinesis phase of the cell cycle. *Curr Biol* 10, 611–614.
- Carreno S, Kouranti I, Glusman ES, Fuller MT, Echard A, Payre F (2008). Moesin and its activating kinase Slik are required for cortical stability and microtubule organization in mitotic cells. *J Cell Biol* 180, 739–746.
- Cheffings TH, Burroughs NJ, Balasubramanian MK (2016). Actomyosin ring formation and tension generation in eukaryotic cytokinesis. *Curr Biol* 26, R719–R737.
- Chen A, Akhshi TK, Lavoie BD, Wilde A (2015). Importin β mediates the spatio-temporal regulation of anillin through a noncanonical nuclear localization signal. *J Biol Chem* 290, 13500–13509.
- Clarke PR, Zhang C (2008). Spatial and temporal coordination of mitosis by Ran GTPase. *Nat Rev Mol Cell Biol* 9, 464–477.
- D'Avino PP, Giansanti M, Petronczki M (2015). Cytokinesis in animal cells. *Cold Spring Harb Perspect Biol* 7, a015834.
- Dechant R, Glotzer M (2003). Centrosome separation and central spindle assembly act in redundant pathways that regulate microtubule density and trigger cleavage furrow formation. *Dev Cell* 4, 333–344.
- Dehapiot B, Carrière V, Carroll J, Halet G (2013). Polarized Cdc42 activation promotes polar body protrusion and asymmetric division in mouse oocytes. *Dev Biol* 377, 202–212.
- Dehapiot B, Halet G (2013). Ran GTPase promotes oocyte polarization by regulating ERM (Ezrin/Radixin/Moesin) inactivation. *Cell Cycle* 12, 1672–1678.
- Deng M, Suraneni P, Schultz RM, Li R (2007). The Ran GTPase mediates chromatin signalling to control cortical polarity during polar body extrusion in mouse oocytes. *Dev Cell* 12, 301–308.
- Frenette P, Haines E, Loloayan M, Kinal M, Pakarian P, Piekny A (2012). An anillin-Ect2 complex stabilizes central spindle microtubules at the cortex during cytokinesis. *PLoS One* 7, e34888.
- Green RA, Paluch E, Oegema K (2012). Cytokinesis in animal cells. *Annu Rev Cell Dev Biol* 28, 29–58.
- Hasegawa K, Ryu SJ, Kaláb P (2013). Chromosomal gain promotes formation of a steep RanGTP gradient that drives mitosis in aneuploid cells. *J Cell Biol* 200, 151–161.
- Hu C, Coughlin M, Field CM, Mitchison TJ (2008). Cell polarization during monopolar cytokinesis. *J Cell Biol* 181, 195–202.
- Kaláb P, Pralle A, Isacoff EY, Heald R, Weis K (2006). Analysis of a RanGTP-regulated gradient in mitotic somatic cells. *Nature* 440, 697–701.
- Kaláb P, Weis K, Heald R (2002). Visualization of a Ran-GTP gradient in interphase and mitotic *Xenopus* egg extracts. *Science* 295, 2452–2456.
- Kim H, Johnson JM, Lera RF, Brahma S, Burkard ME (2017). Anillin phosphorylation controls timely membrane association and successful cytokinesis. *PLoS Genet* 13, e1006511.
- Kiyomitsu T, Cheeseman IM (2013). Cortical dynein and asymmetric membrane elongation coordinately position the spindle in anaphase. *Cell* 154, 391–402.
- Kotadia S, Montembault E, Sullivan W, Royou A (2012). Cell elongation is an adaptive response for clearing long chromatid arms from the cleavage plane. *J Cell Biol* 199, 745–753.
- Lacroix B, Maddox AS (2012). Cytokinesis, ploidy and aneuploidy. *J Pathol* 226, 338–351.
- Lee YP, Wong CH, Chan KS, Lai SK, Koh CG, Li HY (2012). In vivo FRET imaging revealed a regulatory role of RanGTP in kinetochore-microtubule attachments via Aurora B kinase. *PLoS One* 7, e45836.
- Lewellyn L, Dumont J, Desai A, Oegema K (2010). Analyzing the effects of delaying aster separation on furrow formation during cytokinesis in the *Caenorhabditis elegans* embryo. *Mol Biol Cell* 21, 50–62.
- Li HY, Zheng Y (2004). Phosphorylation of RCC1 in mitosis is essential for producing a high RanGTP concentration on chromosomes and for spindle assembly in cells. *Genes Dev* 18, 512–527.
- Liu J, Fairn GD, Ceccarelli DF, Sicheri F, Wilde A (2012). Cleavage furrow organization requires PIP(2)-mediated recruitment of anillin. *Curr Biol* 22, 64–69.
- Mendoza M, Norden C, Durrer K, Rauter H, Uhlmann F, Barral Y (2009). A mechanism for chromosome segregation sensing by the NoCut checkpoint. *Nat Cell Biol* 11, 477–483.
- Nishimoto T, Eilen E, Basilico C (1978). Premature of chromosome condensation in a ts chromatin-mutant of BHK cells. *Cell* 15, 475–483.
- Norden C, Mendoza M, Dobbelaere J, Kotwaliwale CV, Biggins S, Barral Y (2006). The NoCut pathway links completion of cytokinesis to spindle midzone function to prevent chromosome breakage. *Cell* 125, 85–98.
- Oegema K, Savoian MS, Mitchison TJ, Field CM (2000). Functional analysis of a human homologue of the *Drosophila* actin binding protein anillin suggests a role in cytokinesis. *J Cell Biol* 150, 539–552.
- Petronczki M, Glotzer M, Kraut N, Peters JM (2007). Polo-like kinase 1 triggers the initiation of cytokinesis in human cells by promoting recruitment of the RhoGEF Ect2 to the central spindle. *Dev Cell* 12, 713–725.
- Piekny AJ, Glotzer M (2008). Anillin is a scaffold protein that links RhoA, actin, and myosin during cytokinesis. *Curr Biol* 18, 30–36.
- Piekny AJ, Maddox AS (2010). The myriad roles of anillin during cytokinesis. *Sem Cell Dev Biol* 21, 881–891.
- Potapova TA, Daum JR, Pittman BD, Hudson JR, Jones TN, Satinover DL, Stukenberg PT, Gorbisky GJ (2006). The reversibility of mitotic exit in vertebrate cells. *Nature* 440, 954–958.
- Rodrigues NT, Lekomtsev S, Jananji S, Kriston-Vizi J, Hickson GR, Baum B (2015). Kinetochore-localized PP1-Sds22 couples chromosome segregation to polar relaxation. *Nature* 524, 489–492.
- Roubinet C, Decelle B, Chicanne G, Dorn JF, Payrastré B, Payre F, Carreno S (2011). Molecular networks linked by moesin drive remodeling of the cell cortex during mitosis. *J Cell Biol* 195, 99–112.
- Silverman-Gavriila RV, Hales KJ, Wilde A (2008). Anillin-mediated targeting of peanuto pseudocleavage furrows is regulated by the GTPase Ran. *Mol Biol Cell* 19, 3735–3744.
- Soderholm JF, Bird SL, Kaláb P, Sampathkumar Y, Hasegawa K, Uehara-Bingen M, Weis K, Heald R (2011). Importazole, a small molecule inhibitor of the transport receptor importin- β . *ACS Chem Biol* 6, 700–708.
- Somers WG, Saint R (2003). A RhoGEF and Rho family GTPase-activating protein complex links the contractile ring to cortical microtubules at the onset of cytokinesis. *Dev Cell* 4, 29–39.
- Soniati M, Chook YM (2015). Nuclear localization signals for four distinct karyopherin- β nuclear import systems. *Biochem J* 468, 353–362.
- Steigemann P, Wurzenberger C, Schmitz MH, Held M, Guizetti J, Maar S, Gerlich DW (2009). Aurora B-mediated abscission checkpoint protects against tetraploidization. *Cell* 136, 473–484.
- Straight AF, Field CM, Mitchison TJ (2005). Anillin binds nonmuscle myosin II and regulates the contractile ring. *Mol Biol Cell* 16, 193–201.
- Sun L, Guan R, Lee J, Liu Y, Chen M, Wang J, Wu JQ, Chen Z (2015). Mechanistic insights into the anchorage of the contractile ring by anillin and Mid1. *Dev Cell* 33, 413–426.
- Tse YC, Piekny A, Glotzer M (2011). Anillin promotes astral microtubule-directed cortical myosin polarization. *Mol Biol Cell* 22, 3165–3175.
- van Oostende Triplet C, Garcia MJ, Haji Bik H, Beaudet D, Piekny A (2014). Anillin interacts with microtubules and is part of the astral pathway that defines cortical domains. *J Cell Sci* 127, 3699–3710.
- Werner M, Munro E, Glotzer M (2007). Astral signals spatially bias cortical myosin recruitment to break symmetry and promote cytokinesis. *Curr Biol* 17, 1286–1297.
- Yüce O, Piekny A, Glotzer M (2005). An ECT2–centralspindlin complex regulates the localization and function of RhoA. *J Cell Biol* 170, 571–582.
- Zanin E, Desai A, Poser I, Toyoda Y, Andree C, Moebius C, Bickle M, Conrad B, Piekny A, Oegema K (2013). A conserved RhoGAP limits M phase contractility and coordinates with microtubule asters to confine RhoA during cytokinesis. *Dev Cell* 26, 496–510.
- Zhao WM, Fang G (2005). MgcRacGAP controls the assembly of the contractile ring and the initiation of cytokinesis. *Proc Natl Acad Sci USA* 102, 13158–13163.